A Novel Physiologically Based Algorithm (PBA) for Fast CFD Computation of Flow Fractional Reserve (FFR) in Coronary Artery Trees

Sholpan Sumbekova[1], Nurzhan Maldenov[1], Asset Zhamiyev[1], Yang Tianqi[2], Su Xiaohui[2] and Yong Zhao[1]

[1] Mechanical and Aerospace Engineering Department, School of Engineering, Nazarbayev University, Astana 010000, Kazakhstan
[2] School of Hydraulic Engineering, Dalian University of Technology, China 116024

Abstract
A novel physiologically based algorithm (PBA) for fast CFD computation of Flow Fractional Reserve (FFR) in Coronary Artery Trees (CATs) is proposed and developed, which, unlike traditional methods, is based on the extension of the Murray's law for blood vessels at the outlets and extra inlet conditions prescribed alternatively and iteratively. The PBA is then implemented in both SimVascular and Ansys CFD for testing and validation. For validation purpose, 3D models of CATs are built by using their CT images and computational meshes generated for mesh convergence study. Results obtained are then compared with Invasive Coronary Angiographic (ICA) data for validation and evaluation of its accuracy and computational efficiency. The PBA is found to be a robust patient-specific and physiologically sound method that can be a good alternative to the existing Lumped Parameter Model (LPM) which is based on empirical scaling correlations using limited population-averaged data and requires nonlinear iterative computation for convergence.

Keywords: FFR, Blood Flow Simulation, SimVascular, coronal stenosis, cCTA

1. Introduction

A physiologically normally functioning heart can perform 75 cycles per minute on average and sustain continuous blood circulation [2]. The change of coronary artery shape caused by atherosclerosis may result in a reduction of blood flow inside the artery, which in turn, might contribute to the development of abnormal cardiac cycles due to ischemia. The plaque formation on the walls of the coronary arteries increases the possibility of blood flow reduction and may contribute to the progression of coronary artery disease (CAD).

Computer image processing generates geometrical data about the vessels, which enables doctors to identify the vessel obstructions visually. Meijboom et al. [4] have found that Coronary Computed Tomographic angiography (cCTA) for the analysis of CAD often overestimates the clinical severity of geometrical obstructions in coronary vessels, resulting in a true negative rate of 64%.

Spaan et al. [12] have proposed to use Fractional Flow Reserve (FFR) to describe the hemodynamic condition of the cardiovascular system, which is defined as the ratio of the pressure distal to the stenosis to the pressure proximal to it. FFR can be measured directly during the Invasive Coronary Angiography

(ICA) using pressure sensors passing through the guide-catheters and guide-wires [9]. Thus, through this procedure, the difference in pressure values across coronary stenosis regions could be obtained.

Numerous studies have verified the effectiveness of FFR based diagnosis in terms of cost and severity and long-term outcome. For example, Puymirat et al. [10] conducted a clinical study where patients underwent conventional angiography-guided and FFR guided treatments with revascularization. The results showed that FFR based treatment had decreased combined death and non-fatal myocardial infarction by 5.46 times compared to conventional angio- revascularization [10]. They also have noted that FFR based treatment is 31% cheaper than conventional angio-treatment. Pijls et al. [8] studied the functional severity assessment of CAD among patients. It was found that the FFR technique could produce 93% accuracy in prediction of reversible ischemia in a study group of 45 patients. De Bruyne et al. [1] suggested that the implementation of FFR guided Percutaneous coronary intervention (PCI) treatment would decrease the rate of urgent revascularization, where a special stent is inserted in a stenosis-containing artery by a surgeon, in order to enlarge the geometrical obstruction of a vessel under the PCI procedure.

The existing CFD packages that have been clinically tested in large clinical trials are Discover Flow, HeartFlow - NXT and other Platforms for the physiologic assessment of coronary artery function [6]. The use of CFD to estimate FFR (FFR_{CFD}) has been considered as a promising non-invasive substitute of FFR_{ICA} measurement [11]. Many studies demonstrate that the FFR_{CFD} derived from cCTA through CFD simulations has improved the diagnostic accuracy and discrimination than CT alone for the detection of coronary lesions that cause myocardial ischemia, especially for intermediate stenosis [6], which is also much cheaper and non-invasive, thus much less much harmful to the patients compared with ICA.

However, a coronary tree normally has numerous branches, the outflow boundary conditions become almost impossible to be determined experimentally due to their small sizes. Therefore, the Windkessel-type boundary conditions based on the so-called Lumped Parameter Model (LPM), and the more complicated Lumped Parameter Network Model (LPNM) are normally adopted for approximately calculating the outflow boundary conditions which represent the extremely complex dynamic interactions between the tree and its downstream microvasculature [3, 15]. These methods are based on the circuit analogy theory which requires the determination of resistances, capacitances and empirical correlations which are often difficult to calculate without a specific patient's data and are usually not physiologically based. The coupling of the resultant ODEs from these methods with the CFD solver also create ambiguous boundary conditions that may often lead to slow convergence or even divergence in numerical solutions [3, 15].

In this study, we propose an efficient PBA for patient-specific calculation of coronary tree outflow boundary conditions to provide a solution to the above-mentioned difficulties, which can provide realistic and personalized outflow boundary conditions in the absence of measured data, based on an extension of Murray's law and extra inlet conditions [5] to be applied alternatively and iteratively. Vascular systems obey Murray's law, which states that the power for transport and upkeep of blood is minimal in mammalian vascular transport systems, which is employed by the proposed PBA to prescribe the initially boundary conditions, which , in turn, are modified through alternatively applying the extra inlet boundary conditions and iterations towards final numerical convergence.

2. Mathematical Formulations and Numerical Methods

2.1 Governing equations for hemodynamic flow

Simvascular includes a flow solver based on PHASTA (Parallel, Hierarchic, Adaptive, Stabilized, Transient, Analysis) [13], which numerically solve the governing equations for flow in blood vessels. PHASTA is a parallel unstructured grid solver to calculate 3D compressible and incompressible,

laminar and turbulent, steady and unsteady flows. Incompressible 3D Navier-Stokes equations (1) are used to solve blood flow in SimVascular:

$$\rho \dot{v}_i + \rho v_j v_{i,j} - p_{,i} - \tau_{ij,j} = 0,$$
$$v_{i,i} = 0, \quad (1)$$

ρ – density of blood
v_i – i component of flow velocity
$\dot{v}_i$ – velocity derivative with respect to time
p – pressure
τ_{ij} – stress tensor (viscous portion)

Streamline-upwind/Petrov-Galerkin (SUPG) and pressure-stabilizing/Petrov-Galerkin (PSPG) Finite Element Methods are used to discretize the Navier-Stokes equation (1) in space and are integrated in time by an implicit scheme. The resultant algebraic equations are solved bv a so-called preconditioned linear solver (PCLS) [13].

On the other hand, the Ansys CFX solver solves the same Navier-Stokes equations with the Finite Volume Method (FVM) and SIMPLE/SIMPLEC/PISO pressure correction methods for impressible flows [7].

Domain of equation is defined with $\Omega \in \mathbb{R}^3$, and boundary condition are $\Gamma = \Gamma_D \cup \Gamma_N$, where Γ_D is Dirichlet Boundary Condition (BC) and Γ_N Neumann BC. The discretization of Ω is performed with n_{el} linear unstructured tetrahedral elements, $\overline{\Omega}_e$. At the end, eq (1) is transformed into eq (2):

$$B_G(w_i, q; v_i, p) = \int_\Omega \{w_i(\rho \dot{v}_i + \rho v_j v_{i,j}) + w_{i,j}(-\rho \sigma_{ij} + \tau_{ij}) - q_{,i} v_i\} d\Omega + \int_{\Gamma_N} \{w_i(\rho \delta_{in} + \tau_{in}) + q v_{in}\} d\Gamma \quad (2)$$
$$\text{where } w \in W_n^k \text{ and } q \in P_h^k$$

2.2 The Murray's law and PBA for rapid iterative computation of outlet conditions

The methodology proposed in this study aims to provide a solution to the above-mentioned difficulties with Windkessel type boundary conditions, and generate patient-specific realistic outflow boundary conditions in the absence of measured data, based on an extension of the Murray's law [5] and extra inlet conditions prescribed alternatively in iterations. Vascular systems are found to obey Murray's law, which states that the power for transport and upkeep of blood is minimal in a vascular transport system.

According to the Hagen-Poiseuille Law for laminar flow in a vessel, the power required to drive a blood flow through it is

$$P_t = \frac{8\mu l}{\pi r^4} \dot{Q}^2 \quad (3)$$

where $\dot{Q}$ is the volumetric flow rate, l the length of the vessel, r its radius and μ the blood viscosity.

Furthermore, the power necessary for the maintenance of the blood in the vessel is proportional to the blood volume in the vessel:

$$V = \pi l r^2 \quad (4)$$

The power required to maintain the metabolism in the blood is thus

$$P_m = \lambda V = \lambda \pi l r^2 \tag{5}$$

where λ is the metabolic rate of the blood.

The total power required to drive the blood and maintain it is

$$P = P_t + P_m = \frac{8\mu l}{\pi r^4}\dot{Q}^2 + \lambda \pi l r^2 \tag{6}$$

The radius that meets the minimum power requirement is obtained through the differentiation of *P* with respect to *r* and setting it to zero:

$$\frac{dP}{dr} = -\frac{32\mu l}{\pi r^5}\dot{Q}^2 + 2\lambda \pi l r = 0 \tag{7}$$

Thus,

$$\dot{Q} = \frac{\pi}{4} r^3 \sqrt{\frac{\lambda}{\mu}} \tag{8}$$

This functional relationship exists between vessel radius and volumetric flow rate in individual vessels. A novel iterative scheme is thus proposed to couple the Murray's law with CFD simulation to search for the converged patient-specific flow outlet conditions for all the outlets of a coronary tree for given inlet pressure and volumetric flow rate which are prescribed alternatively through iterative computation.

For a particular branch *i* of a coronary tree with *N* branches its outflow is

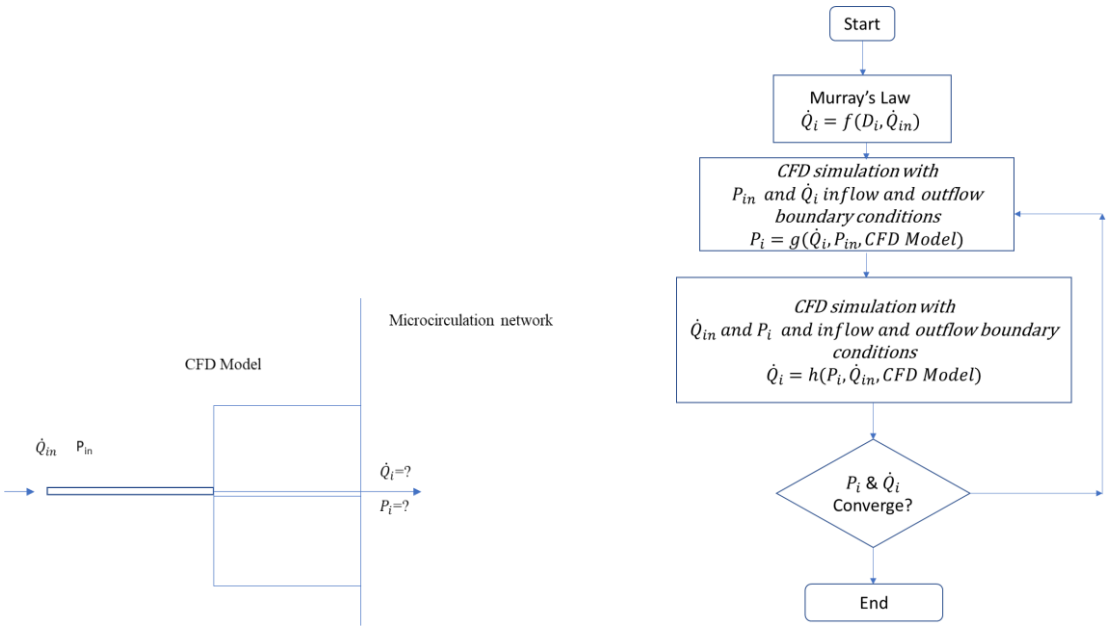

a). b).

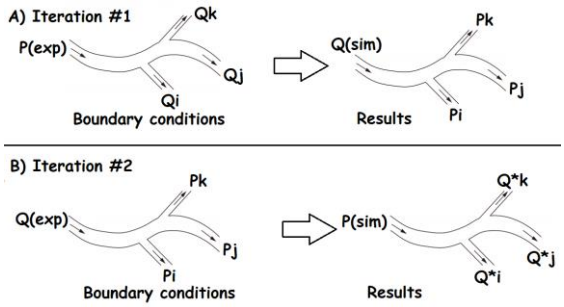

c).

Figure 1. a) schematic of the new boundary model, b) algorithm for the outflow boundary conditions, c) iterative procedure of the algorithm

$$\dot{Q}_i = \frac{\pi}{4} r_i^3 \sqrt{\frac{\lambda}{\mu}} \tag{9}$$

And according to the conservation law, we have

$$\dot{Q}_{in} = \sum_{i=1}^{N} \dot{Q}_i \tag{10}$$

$$\dot{Q}_i = \frac{r_i^3}{r_{in}^3} \dot{Q}_{in} \tag{11}$$

Our new physiologically based algorithm (PBA) to extract personalized/patient-specific outflow boundary conditions that represent the interactions between the coronary tree and its micro circulation

network downstream under both steady and unsteady conditions are shown in a flowchart as illustrated in Figure 1 b-c.

In this work the above-mentioned methods are implemented in both SimVascular and Ansys CFX to perform computational study of the hemodynamics in a number of patient specific geometries with the aim of validating the methods using related ICA measurements, such as inlet flow rate and pressure and FFR_{ICA}. There are four vascular cases, named as CT209, CT14, CHN03 and CHN13 implemented by using the proposed PBA. Table 1 lists the workflow procedure for the PBA.

Table 1. Workflow procedure of Rapid Iterative algorithm.

		Inlet	Outlets			
1st round of iteration	Input to CFD Solver	P_{exp}[a]	Q_1	Q_2	…	Q_n
			**calculated by Murray's law at beginning*			
	The output from CFD Solver	Q_{ss}	P_1^{ss}	P_2^{ss}	…	P_n^{ss}
	Input to CFD solver	Q_{exp}[b]	P_1^{ss}	P_2^{ss}	…	P_n^{ss}
	Output from CFD Solver	P_{ss}	Q_1^{ss}	Q_2^{ss}	…	Q_n^{ss}
2nd round of iteration	Input to CFD solver	P_{exp}	Q_1^{ss}	Q_2^{ss}	…	Q_n^{ss}
	Output from CFD solver	Q_{ss}	P_1^{ss}	P_2^{ss}	…	P_n^{ss}
	Input to CFD solver	Q_{exp}	P_1^{ss}	P_2^{ss}	…	P_n^{ss}
	Output from CFD solver	P_{ss}	Q_1^{ss}	Q_2^{ss}	…	Q_n^{ss}
Nth round of iteration	-	-	-	-	-	-

[a] Experimentally measured distal pressure at the inlet of blood vessel.
[b] Experimentally measured flow rate at the inlet of blood vessel.

$Q_{ss}; P_{ss}; Q_n^{ss}; P_n^{ss}$ – CFD solver calculated values of pressure and flow rate at the inlet and outlets at different stages.

The geometries and their outlets of CT209, CHN13, CT14 and CHN03 are presented in Figure 2 a-d. Table 2 shows the experimental values of pressure and flow rate at the inlet (aorta) of a vessel that is obtained for CT209, CHN13, CT14 and CHN03, respectively, while Table 3 shows the calculated initial flow rates at the outlets for the four models, which are calculated using equation (11) which is based on Murray's law. Inlet and outlet boundary conditions are prescribed according to Table 1.

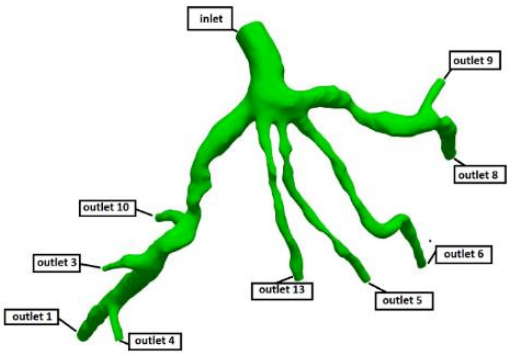

a). *CT209 model*

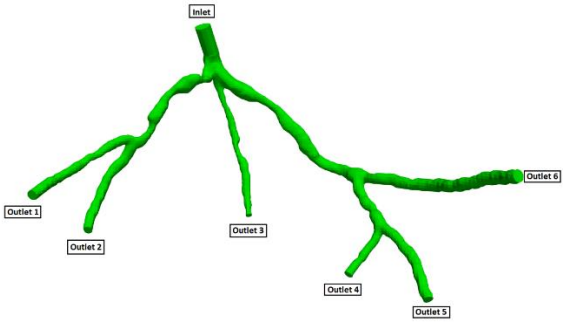

b). CHN13 model

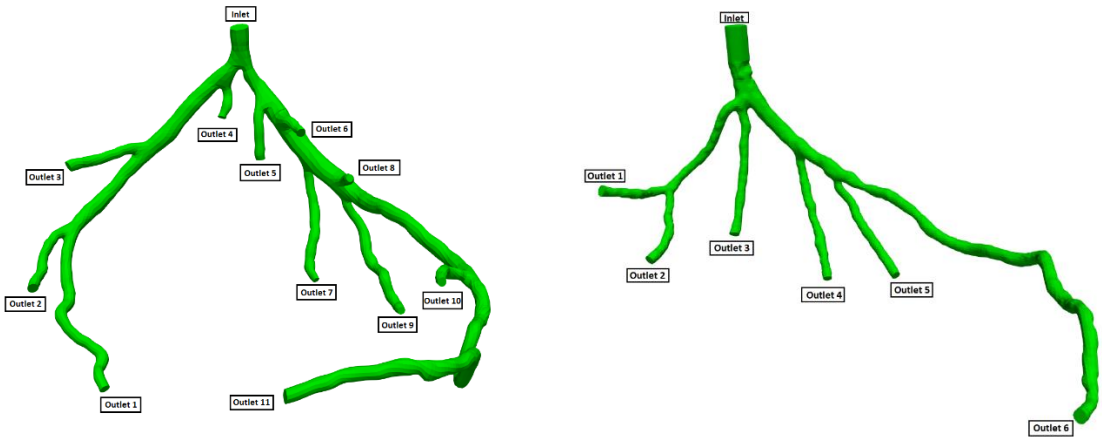

c). CT14 model d). CHN03 model

Figure 2. Geometry and outlets of the tested models

Table 2. Experimentally obtained input parameters for simulation for tested models

Parameter\Model	CT209	CHN13	CT14	CHN03
Inlet pressure in mmHg (Pa)	90.53 (12070.12)	90.61 (12870.12)	76.8 (10240.80)	76.5 (10201.90)
Inlet flow rate in cm^3/s	9.40	7.18	6.19	6.18

Table 3. Initial calculated flow rates at each outlet by Murray's law for all models

Murray's law calculation for outlet flow rates for model CT209						
	i	A_i (cm^2)	d_i (cm)	d_i^3 (cm^3)	α_i	Q_i (cm^3/s)
outlet 1	1	4.114	2.289	11.988	0.315	2.965
outlet 3	2	0.568	0.851	0.616	0.016	0.152
outlet 4	3	0.925	1.085	1.279	0.034	0.316
outlet 5	4	0.977	1.116	1.388	0.037	0.343
outlet 6	5	1.802	1.515	3.475	0.091	0.859
outlet 8	6	4.105	2.286	11.948	0.314	2.955
outlet 9	7	1.674	1.460	3.111	0.082	0.769
outlet 10	8	1.173	1.222	1.824	0.048	0.451
outlet 13	9	1.398	1.334	2.374	0.062	0.587

Murray's law calculation for outlet flow rates for CHN13						
	i	A_i (cm^2)	d_i (cm)	d_i^3 (cm^3)	α_i	Q_i (cm^3/s)
outlet 1	6	2.712	1.858	6.418	0.227	1.630

outlet 2	1	1.832	1.527	3.564	0.126	0.905
outlet 3	3	1.005	1.131	1.447	0.051	0.368
outlet 4	2	1.950	1.576	3.913	0.139	0.994
outlet 5	5	1.969	1.583	3.970	0.141	1.009
outlet 6	4	3.382	2.075	8.936	0.316	2.270

Murray's law calculation for outlet flow rates for CT14						
	i	A_i (cm^2)	d_i (cm)	d_i^3 (cm^3)	α_i	Q_i (cm^3/s)
outlet 1	1	2.0253	1.6058	4.1410	0.1008	0.6238
outlet 2	2	2.5091	1.7874	5.7102	0.1390	0.8602
outlet 3	3	2.8210	1.8952	6.8072	0.1657	1.0254
outlet 4	4	1.8029	1.5151	3.4779	0.0846	0.5239
outlet 5	5	1.9039	1.5570	3.7744	0.0919	0.5686
outlet 6	6	2.2769	1.7026	4.9359	0.1201	0.7436
outlet 7	7	1.2534	1.2633	2.0160	0.0491	0.3037
outlet 8	8	1.0056	1.1315	1.4487	0.0353	0.2182
outlet 9	9	1.2546	1.2639	2.0189	0.0491	0.3041
outlet 10	10	1.3891	1.3299	2.3522	0.0572	0.3543
outlet 11	11	2.11181	1.6398	4.4091	0.1073	0.6642

Murray's law calculation for outlet flow rates for CHN03						
	i	A_i (cm^2)	d_i (cm)	d_i^3 (cm^3)	α_i	Q_i (cm^3/s)
outlet 1	1	2.5675	1.8081	5.9106	0.2240	1.3847
outlet 2	2	2.2262	1.6836	4.7721	0.1808	1.1179
outlet 3	3	2.1930	1.6710	4.6658	0.1768	1.0930
outlet 4	4	1.8206	1.5225	3.5293	0.1338	0.8268
outlet 5	5	1.7784	1.5048	3.4074	0.1291	0.7982
outlet 6	6	2.0126	1.6008	4.1021	0.1555	0.9610

The convergence criteria is evaluated at the end of each iteration with equation (12). The procedure presented in Table 1 is repeated continuously until the convergence is achieved.

$$\frac{|P_{ss}-P_{exp}|}{P_{exp}} = \delta \leq 0.1\% \tag{12}$$

$$\Delta P = \frac{|P_{calculated}-P_{experimental}|}{P_{calculated}} \times 100\% \tag{13}$$

$$\Delta Q = \frac{|Q_{calculated}-Q_{experimental}|}{Q_{calculated}} \times 100\% \tag{14}$$

$$FFR = \frac{\min(P_1^{SS},P_2^{SS},\ldots P_n^{SS})}{P_{exp}} \tag{15}$$

3. Results and Discussion

Mesh generation is performed using the open source TetGen kernel and MeshSim, which generate volumetric meshes in the blood vessels. In particular, TetGen is capable of generating tetrahedral

meshes for a diverse variety of geometries automatically. Ansys MESH, a commercial software, is used to generate meshes for simulations using Ansys CFX.

Estimated minimum mesh size for each mesh is about a half of the radius of the smallest artery (inlet/outlet) present in the model. Estimated mesh size for the coronary artery tree model CT209 is 0.1702, and for CHN13 it is 0.2262. The convergence criteria of $\frac{|P_{ss}-P_{exp}|}{P_{exp}} = \delta \leq 0.1\%$ for inlet pressure, defined in equation (12), is used for all computations. The percentage relative difference of calculated and experimental FFR is used as a degree of deviation from experimentally obtained FFR.

There are four sets of meshes generated for CT14 (with mesh cell numbers as: 118,874, 231,930, 486,447, 1,052,529) and five sets of meshes for CHN03 (with mesh element numbers as: 69,681, 139,833, 286,897, 406,606, 779,482) to study mesh convergence. When the grid number is increased from 100,000 to about 1.05 million, the change value of the distal pressure is less than 5% (about 2.2%). After mesh dependency test, the model was discretized with a total of about 0.5 million volume cells. Further grid refinement leads to < 1% relative error.

Pressure and velocity residuals at all the outlets are defined as the averages of relative percentage differences in consecutive iterations. The convergence of CFD simulation can be monitored by examining the reduction of the values of the pressure and flow rate residuals at the outlets as well. Figs. 11 and 12 show pressure and flow rate residuals at the outlets for CT209, respectively, for all iterations where residual values are plotted in logarithmic scale. Mesh sizes of 0.1702 and 0.20 have the same fluctuation behaviors for all round of iterations. Minimum pressure residual values of 1.93E-7 and 2E-7 are observed for both meshes, whereas the maximum values are 3.62E-7 and 4.43E-7 respectively.

FFR is calculated using equation (15). The experimental value of FFR is 0.76 for CT209 model [13]. The percentage relative difference of FFR values of 0.20% and 0.34% are recorded for the mesh sizes of 0.1702 and 0.20, respectively. Zhang et al. [14] have computed non-invasive FFR value of 0.73 whereas experimental (ICA) FFR is about 0.76 for CT209 model. The final values of FFR for mesh sizes of 0.1702 and 0.20 are FFR=0.758 and FFR=0.757 which agree very well with the ICA FRR.

The location of Left Anterior Descending (LAD) Proximal artery is indicated as artery stenosis region for CT209 model in Zhang et al. [14]. The dark blue region of the blood vessel is LAD Proximal (Figure 3a). Therefore, it is found that the artery stenosis is located in the same region as it was observed by Zhang et al. [14]. The visualization of velocity streamlines shows an increase in velocity magnitude in the stenotic region and several possible stenosis locations as seen on the Figure 3 b.

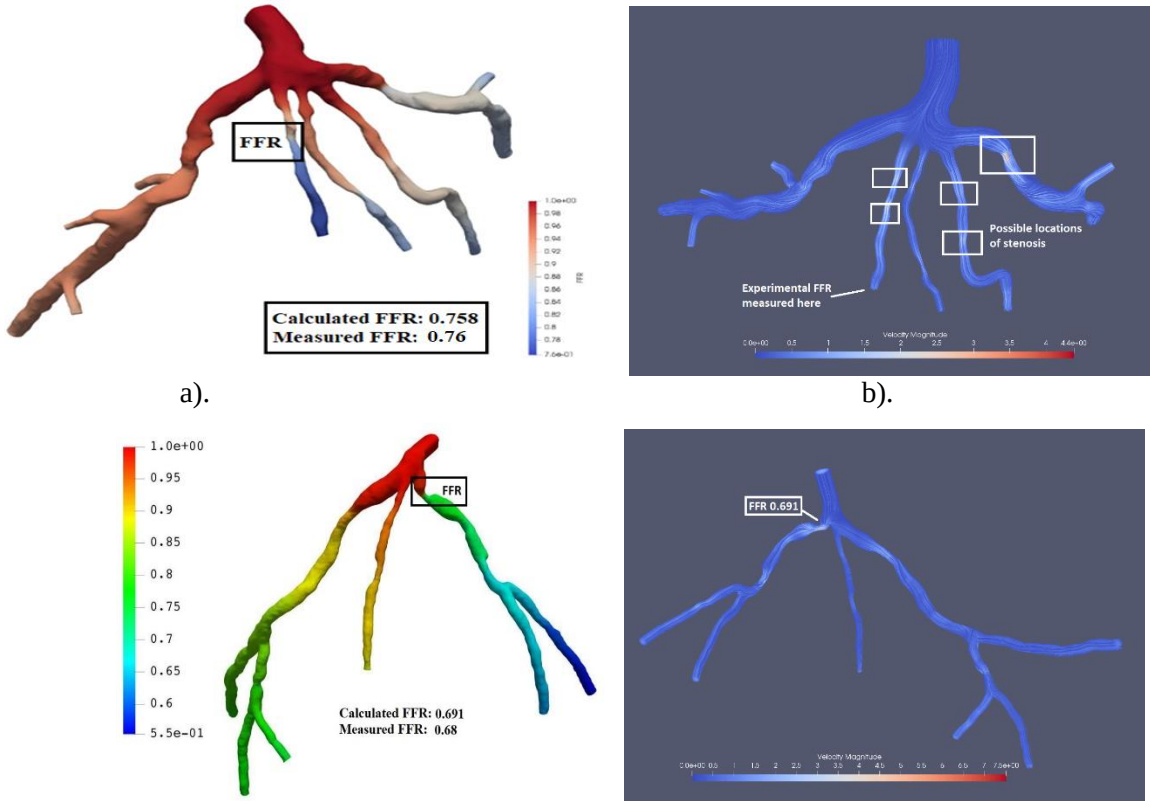

Figure 3 a). FFR distribution along with the shape of CT209 model, b). Visualization of velocity streamlines in the CT 209 model, c). FFR distribution along with the shape of CT209 model, d). Visualization of velocity streamlines in the CT 209 model. Simvascular results.

The simulations of blood flow in the model CHN13 are performed using three mesh sizes (coarse, fine and very fine). The relative differences of inlet flow rates for all three mesh sizes are less than 1% with a maximum of 0.02% observed for the finest mesh. The experimental FFR for the CHN13 model is 0.68. The results show that the finest mesh size (0.22) produces the closest to this value. FFR obtained from the simulations with the finest mesh size is equal to 0.691.

We carried out the comparison between the results obtained by traditional lumped parameter method and those obtained by the current method as well as the ICA measurement. It is found that the current method demonstrates better accuracy and efficiency than the traditional methods. The calculated FFRs for CT14 and CHN03 by the PBA are 0.975 and 0.691, which is in excellent agreement with the corresponding experimental values of 0.97 and 0. 68 respectively.

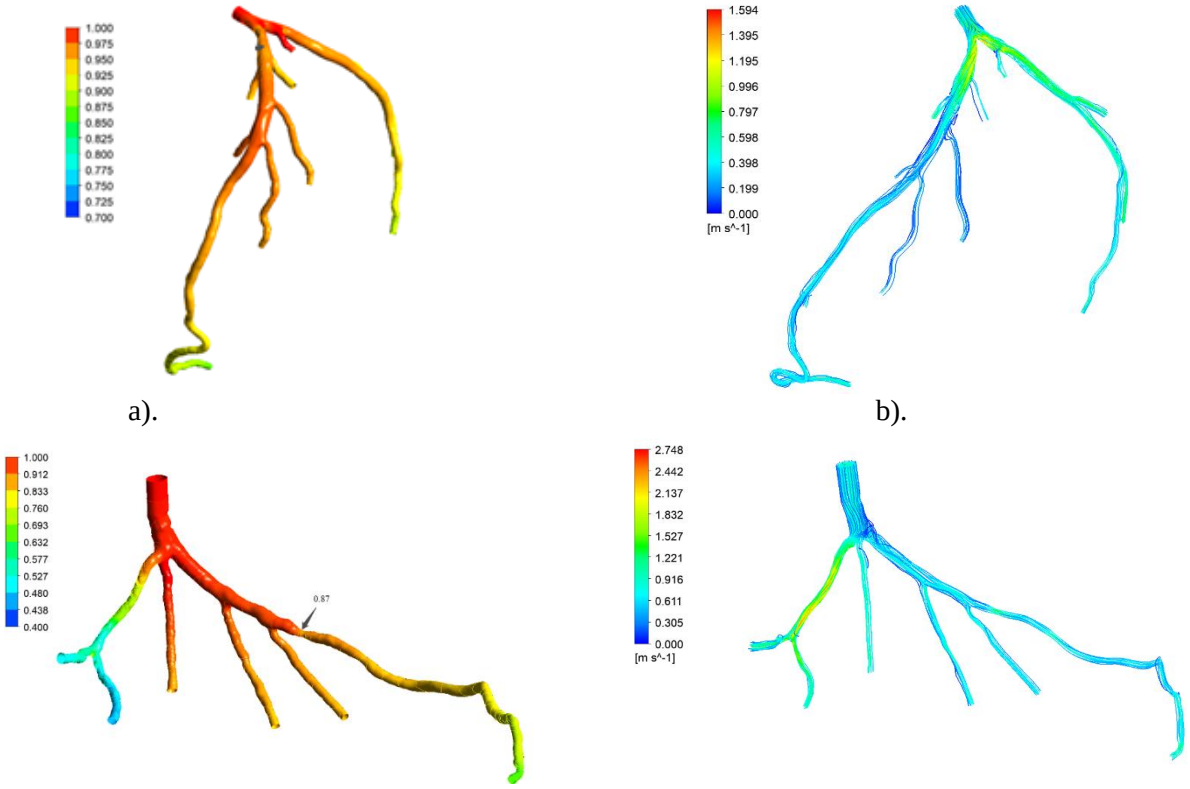

Figure 4. FFR distribution along with the shape of CT14 model, b). Visualization of velocity streamlines in the CT14 model, c). FFR distribution along with the shape of CHN03 model, d). Visualization of velocity streamlines in the CHN03 model. Ansys results.

Table 4. Relative errors calculated between the invasive and calculated FFRs by both Simvascular and Ansys CFX

model	Calculated FFR		Invasive FFR	Relative error, %	
	Ansys CFX	Simvascular		Ansys CFX	Simvascular
CT209	0.753	0.758	0.76	0.92	0.26
CT14	0.96	0.97	0.975	1.54	0.51
CHN03	0.87	0.872	0.86	1.16	1.40
CHN13	0.658	0.691	0.68	3.24	1.62

A summary of the comparison of the calculated and experimental ICA FFRs are presented in the Table 4. The results show that the differences between the relative errors for Ansys and Simvascular is at most of 3.24%. This shows that the proposed PBA produces results that are solver independent.

Further validation of the PBA method is performed using traditional LPM method described in the paper by Zhang et al [14] for model CT14. The LPM method uses a reference pressure, resistances at every outlet representing the flow resistance from the downstream microvasculature, an overall resistance for the whole CAT which is related to the outlet resistances through an population-averaged

empirical scaling law [14], and an iterative procedure to calculate the resistances and reference pressure, thus resulting in the outlet pressures in each branch outlet. Three simulations were run for the model CT14 using both methods: the traditional LPM method is run using Ansys, while the proposed PBA is used in Simvascular. Table 5 compares the flow rates at the outlets, which show that the percentage deviations between the flow rates obtained using PBA and LPM are below 0.1%, yielding on average 0.036%.

It is found that the LPM cannot always guarantee convergence to a unique solution for every case, while the proposed PBA can generate convergence to accurate solutions for all the four cases studied. This shows that the PBA is far more robust than the LPM because the former is physiologically based and patient specific while the latter is not!

Table 5. The values of flow rate in each branch of the model CT14 calculated using traditional RCR method and novel PBA method.

Outlet	Q_i(RCR)	Q_i(PBA)	Difference, %
outlet 1	0.6224	0.6224	0.0042
outlet 2	0.8534	0.8535	0.0175
outlet 3	1.0260	1.0260	0.0066
outlet 4	0.5205	0.5200	0.1005
outlet 5	0.5733	0.5734	0.0023
outlet 6	0.7437	0.7431	0.0827
outlet 7	0.3051	0.3050	0.0275
outlet 8	0.2200	0.2199	0.0559
outlet 9	0.3077	0.3076	0.0143
outlet 10	0.3560	0.3559	0.0233
outlet 11	0.6623	0.6627	0.0566

4. Conclusion

In this study, blood flow has been simulated in four coronary artery tree models using a proposed physiologically based algorithm (PBA) implemented in both Simvascular and Ansys CFX CFD solvers, in order to evaluate the performance of the PBA in different CFD solvers.. The boundary conditions at the outlets are obtained with the proposed approach based on Murray's law with excess inlet conditions prescribed alternatively and interactively. Mesh convergence studies are conducted to investigate the sensitivity of the method to the change in mesh sizes. The simulations provided accurate values of FFR both by Simvascular and Ansys CFX. The values of FFR obtained from the simulations using the proposed PBA agree very well with the experimental ICA results [14]. The validation and comparison of the traditional and proposed methods show a flow rate relative difference of 0.1% at most. Compared with the traditional method that may not always ensure convergence to an unique solution for every case, the proposed method always guarantee fast convergence to accurate solution for each and every case. Therefore this non-invasive FFR estimation with the PBA is found to be a promising procedure for clinical patient-specific diagnosis of coronary stenosis, which is much simpler and more efficient than the traditional Windkessel circuit analogy approach. Our analysis also suggests that the proposed PBA combined with an efficient CFD solver can be used as a low cost, efficient and accurate method for patient-specific CAD diagnosis that could potentially serve as an alternative to the costly and harmful invasive coronary angiography (ICA) procedure. Future work on using the PBA for pulsatile flows in CATs with fluid structure interaction is suggested.

5. Acknowledgement

The authors would like to acknowledge the assistance and supply of the NT209, CT14 and CHN03 models by Dr. Zhong Liang as reported in [14]. This work has been supported by the grant project 110119FD4526 "Clustering and settling of inertial particles: fluid-structure interactions approach" awarded within Faculty Development Competitive Research Grant Program 2019-2021 of Nazarbayev University.

8. References

1. De Bruyne B et al. 2012. "Fractional Flow Reserve–Guided PCI versus Medical Therapy in Stable Coronary Disease". *New England Journal of Medicine* 367 (11): 991-1001. Massachusetts Medical Society. doi:10.1056/nejmoa1205361.
2. Gersh Bernard J 2000. *Mayo Clinic Heart Book.* New York: William Morrow. pp. 6–8. ISBN 0-688-17642-9.
3. Kim H J, Vignon-Clementel I E, Coogan J S, Figueroa C A, Jansen K E, and Taylor C A 2010. Patient-specific modeling of blood flow and pressure in human coronary arteries. *Annals of biomedical engineering*, 38(10), 3195-3209.
4. Meijboom W B et al. 2008. Diagnostic Accuracy of 64-Slice Computed Tomography Coronary Angiography. *Journal of the American College of Cardiology* 52 (25): 2135-2144. Elsevier BV. doi:10.1016/j.jacc.2008.08.058.
5. Murray C D 1926. The Physiological Principle of Minimum Work: I. The Vascular System and the Cost of Blood Volume. *Proceedings of the National Academy of Sciences of the United States of America*. 12 (3): 207–214. doi:10.1073/pnas.12.3.207. PMC 1084489. PMID 16576980
6. Nørgaard B L et al. 2014. Diagnostic performance of noninvasive fractional flow reserve derived from coronary computed tomography angiography in suspected coronary artery disease: the NXT trial (Analysis of Coronary Blood Flow Using CT Angiography: Next Steps). *Journal of the American College of Cardiology*, 63(12), 1145-1155.
7. Patankar, S. V. (1980). Numerical Heat Transfer and Fluid Flow. Taylor & Francis. ISBN 978-0-89116-522-4.

8. Pijls N H, De Bruyne B, Peels K, Van Der Voort P H, Bonnier H J, Bartunek J, and Koolen J J 1996. Measurement of fractional flow reserve to assess the functional severity of coronary-artery stenoses. *New England Journal of Medicine*, 334(26), 1703-1708.
9. Pijls Nico H J and Sels Jan-Willem E M 2012. "Functional Measurement of Coronary Stenosis". *Journal of the American College of Cardiology* 59 (12): 1045-1057. Elsevier BV. doi:10.1016/j.jacc.2011.09.077.
10. Puymirat E, Peace A, Mangiacapra F, Conte M, Ntarladimas Y, Bartunek J, Vanderheyden M, Wijns W, De Bruyne B, and Barbato E 2012. "Long-Term Clinical Outcome After Fractional Flow Reserve–Guided Percutaneous Coronary Revascularization in Patients With Small-Vessel Disease". *Circulation: Cardiovascular Interventions* 5 (1): 62-68. Ovid Technologies (Wolters Kluwer Health). doi:10.1161/circinterventions.111.966937.
11. Secchi F et al. 2016. Fractional flow reserve based on computed tomography: an overview. *European Heart Journal Supplements* 2016 18 (Supplement E), E49–E56,doi:10.1093/eurheartj/suw014
12. Spaan J A, Piek J J, Hoffman J I, and Siebes M 2006. "Physiological Basis of Clinically Used Coronary Hemodynamic Indices". *Circulation* 113 (3): 446-455. Ovid Technologies (Wolters Kluwer Health). doi:10.1161/circulationaha.105.587196.
13. Updegrove A, Wilson, N M, Merkow, J, Lan, H, Marsden, A. L, & Shadden, S C. 2017. SimVascular: an open source pipeline for cardiovascular simulation. Annals of biomedical engineering, 45(3), 525-541.
14. Zhang J M et al. 2016. "Simplified Models of Non-Invasive Fractional Flow Reserve Based on CT Images". PLOS ONE 11 (5): e0153070. *Public Library of Science (PLoS)*. doi:10.1371/journal.pone.0153070.
15. Zhong L, Zhang J M, Su B, San Tan R, Allen J C, and Kassab G S 2018. Application of patient-specific computational fluid dynamics in coronary and intra-cardiac flow simulations: Challenges and opportunities. *Frontiers in physiology*, 9.